ISSN 1054-660X, Laser Physics, 2009, Vol. 19, No. 8, pp. 1743–1752.

Relativistic Nonperturbative Above-Threshold Phenomena in Strong Laser Fields

C. Müller*, K. Z. Hatsagortsyan, M. Ruf, S. J. Müller, H. G. Hetzheim, M. C. Kohler, and C. H. Keitel*****

Max-Planck-Institut für Kernphysik, Saupfercheckweg 1, Heidelberg, 69117 Germany

*e-mail: c.mueller@mpi-hd.mpg.de
**e-mail: k.hatsagortsyan@mpi-hd.mpg.de
***e-mail: keitel@mpi-hd.mpg.de

Received February 13, 2009

Abstract—Relativistic features of various nonperturbative above-threshold phenomena in strong laser fields are discussed and compared. This includes above-threshold ionization of multiply charged ions as well as pair production in an ultrastrong laser wave, superimposed with either a nuclear Coulomb field or another counterpropagating laser wave. For the probability of above-threshold pair production, a new scaling relation is given. Particular attention is paid to similarities among these processes, regarding the energy and angular spectra of the particles as well as the total reaction rates.

PACS numbers: 12.20.Ds, 32.80.Rm, 32.80.Wr, 42.50.Hz

DOI: 10.1134/S1054660X09150316

1. INTRODUCTION

Above-threshold phenomena are characteristic for non-perturbative laser-matter interactions [1–5]. Above-threshold ionization (ATI) of atoms was discovered experimentally 30 years ago [6]. Nikolai Borisovich Delone, one of the founders of strong-field multiphoton physics, has played an essential role in clarifying the physics of ATI phenomena.

The fact that the processes of strong-field ionization and pair production share common properties has been realized already in the early stages of their investigation [7, 8]. In both cases, an electron driven by a strong oscillatory electromagnetic field has to travel through a classically forbidden region to reach the continuum. In the ionization case, the forbidden energy gap $\Delta\varepsilon = I_p$ is the ionization potential, while in the case of pair production it is the gap $\Delta\varepsilon = 2mc^2$ between the negative and positive energy continua. Here, m is the electron mass and c the speed of light. Both processes necessarily possess a multiphoton nature, when the photon energy of the driving laser field is less than the forbidden energy gap, $\Delta\varepsilon > \hbar\omega$. As the electron in the presence of the laser field should be born in the continuum with an oscillatory energy U_p (ponderomotive energy), the above-threshold process becomes possible if the ponderomotive energy exceeds the photon energy, $U_p/\hbar\omega > 1$. A more exact ATI parameter, $(U_p/\hbar\omega)(I_p/\hbar\omega)^{1/3} \sim E^2/\omega^{10/3}$, has been derived in [4] (see also [9]) by estimating the ratio of the $n+1$ to the n-photon ionization probability within the WKB approximation; E denotes the laser peak field strength. During the above-threshold process the electron absorbs more photons than required to overcome the gap $\Delta\varepsilon$, which leads to a series of peaks in the photoelectron kinetic-energy spectrum, separated by a photon energy. The borderline to the nonperturbative regimes is marked by the value of the Keldysh parameter γ [10]. The latter can be represented as the energy which the electron absorbs in the laser field during its motion along the typical length l in units of the photon energy: $1/\gamma = eEl/\hbar\omega$, where e is the electron charge. In the ionization case, the typical length is determined by the atomic size a, resulting in $\gamma = \sqrt{I_p/2U_p}$, and in the pair production case, by the Compton wave length $\lambda_C = \hbar/mc$, leading to $1/\gamma = eE/mc\omega \equiv \xi$. While probabilities for multiphoton processes at $\gamma \gg 1$ allow for a perturbation series expansion in powers of γ^{-1}, the nonperturbative above-threshold processes emerge at $\gamma \approx 1$. The Keldysh parameter determines also the quasi-static regime of the interaction. This becomes clear when it is expressed via the tunneling time τ as $\gamma = \omega\tau$. Consequently, for smaller values of the Keldysh parameter, $\gamma \ll 1$, the laser electric field appears quasi-static and the electron release occurs via tunneling through a quasi-static barrier. This regime admits a simple analytical description by the ADK model for ATI [11, 12] and by an analogous tunneling model for pair production [7]. Non-perturbative above-threshold processes at $\gamma \sim 1$ represent an intermediate coupling regime, whose theoretical description is not simple even within the strong-field approximation (SFA) [10, 13]. A specific feature of ATI can be highlighted in contrast with the pair production: in rather strong laser fields the photoelectron spectrum is not confined to energies of direct ATI photoelectrons but extends over a plateau

region which is due to laser-driven electron recollisions with the ionic core [14].

With the availability of superintense laser fields, possessing intensities above 10^{18} W/cm^2 in the near-optical frequency range, laser-atom interaction has entered the relativistic domain [15]. A free electron in an external laser field is accelerated to velocities close to the speed of light when the relativistic laser parameter ξ approaches or exceeds unity. This corresponds to ponderomotive energies $U_p = \frac{1}{4}mc^2\xi^2$ on the order of the electron rest energy. Accordingly, the relativistic mass correction terms are proportional to ξ^2. However, the signature of the relativistic Lorentz force can already be observed in the weakly relativistic regime $\xi < 1$ [16]. In fact, the drift of the ionized electron in the laser propagation direction due to the laser magnetic field can be important if the drift distance $d \sim (c/\omega)\xi^2/2$ is comparable with the electron wave packet size at the moment of recollision. The estimation of this condition shows that the relativistic drift effect is visible already at $\xi \approx 0.15$ with infrared frequencies (laser intensities of order of 10^{17} W/cm^2) [17]. Spin effects in the dynamics are generally smaller, being proportional to $\sim\xi\hbar\omega/mc^2$ (see estimation in [18]). They can, however, induce splitting of radiation lines [19] and spin-flip effects [20].

The SFA has been generalized to the relativistic domain [21] and employed for calculations of the relativistic direct ionization rate of hydrogen-like atoms in strong laser fields [22]. The ADK theory also has been extended to the relativistic regime [23, 24]. Simple analytical expressions for the angular and energy distributions of direct photoelectrons in the relativistic regime have been obtained in [25] by means of the adiabatic Landau–Dykhne approximation. Relativistically strong laser fields have recently been employed in experimental studies on ionization of atoms [26] and molecules [27].

A genuinely relativistic effect is the field-induced generation of electron-positron pairs from vacuum, which is familiar from high-energy photoabsorption in the Coulomb field of nuclei [28] and heavy-ion collision experiments [29]. The Bethe–Heitler process has been observed with γ-photons in targets with a high nuclear charge [30, 31]. The only observation of laser-induced pair production until now was accomplished at SLAC (Stanford, USA) in the multiphoton regime, where an electron beam was brought into collision with an intense optical laser pulse [32]. In this experiment, a γ-photon produced via Compton scattering or the electron Coulomb field assisted the laser beam in the pair production. The similarity between ATI and electron-positron pair production by a laser and a Coulomb field can be traced in the intensity dependence of the process probabilities as well as in the electron spectra. Especially one may emphasize the dependence of the above-threshold spectra on the laser polarization: in a linearly polarized laser field the electron spectra are peaked at zero kinetic energy, whereas in the circular-polarization case a maximum appears when the kinetic energy equals the ponderomotive energy and the particles are most probably created with a large transversal (with respect to the laser propagation direction) momentum $p_\perp \sim mc\xi$ and an even larger longitudinal one $p_z \sim mc\xi^2$. Interestingly, these features in the energy and angular distribution of the created electrons mainly reflect the classical dynamics of an electron, initially born at rest, in an external laser field.

In this contribution we survey various nonperturbative above-threshold processes in the presence of relativistically strong laser fields. Section 2 is devoted to strong-field ionization of hydrogen-like atomic systems. First we describe relativistic effects in ATI spectra (Section 2.1). Apart from their fundamental significance, these effects are also interesting from a practical point of view (Section 2.2). Section 3 deals with the creation of electron-positron pairs in ultrastrong laser fields. Considering pair creation in the combined fields of a proton and a laser beam, we derive a scaling relation for the total production probability in the above-threshold domain (Section 3.1). Besides, above-threshold pair production (ATPP) in the field of two counterpropagating laser pulses is studied, with a focus on effects arising from the laser magnetic-field component. We finish with a conclusion where we draw a comparison between ATI and ATPP. Atomic units (au) are applied in Section 2 unless indicated otherwise.

2. ABOVE-THRESHOLD AND OVER-BARRIER IONIZATION OF ATOMS

2.1. Relativistic Effects in Above-Threshold Ionization

We discuss the main distinguishing features of photoelectron energy spectra and angular distribution in the relativistic regime of ATI. The most conspicuous relativistic feature in the distribution of direct photoelectrons is the change of angular distribution with respect to that of the nonrelativistic case. This is already indicated in the classical description of the ionized electron in the laser field. The electron oscillates not only in the polarization direction x but also drifts in the propagation direction z in the laser field, with the corresponding momentum components and the energy given by

$$p_x = \frac{e}{c}[A(\eta_0) - A(\eta)];$$

$$p_z = \frac{e^2}{2mc^3}[A(\eta_0) - A(\eta)]^2; \quad (1)$$

$$\varepsilon = mc^2 + \frac{e^2}{2mc^3}[A(\eta_0) - A(\eta)]^2,$$

when the electron in the continuum has vanishing initial velocity. Here, η_0 denotes the initial phase of the laser vector potential $A(\eta)$. After the laser field is switched off $A(\eta) \longrightarrow 0$, the electron energy and momenta are:

$$p_x = \frac{eA(\eta_0)}{c}; \quad p_z = \frac{e^2A(\eta_0)^2}{2mc^3}; \qquad \varepsilon - mc^2 = \frac{e^2A(\eta_0)^2}{2mc^2}. \tag{2}$$

Therefore, the electron emission angle along the propagation direction, θ, depends on the value of the vector potential at the ionization moment $A(\eta_0)$: $\theta = \arctan(eA(\eta_0)/2mc^2)$. The kinetic energy of the ionized electron is also determined by $A(\eta_0)$: $\varepsilon_{kin}/U_p = 2(A(\eta_0)/A_0)^2$, where A_0 is the amplitude of the vector-potential. In Fig. 1, the results of a quantum mechanical calculation are shown for the energy and angle resolved spectrum of directly ionized electrons. The calculation employs the relativistic SFA based on the Klein–Gordon equation, which is compared with the nonrelativistic result from the Schrödinger equation within the dipole approximation. We consider a highly relativistic regime with an infrared laser intensity of $I = 1.4 \times 10^{19}$ W/cm^2 ($\omega = 0.05$ au, $\xi \approx 3$).

One can see that in the nonrelativistic description the distribution is symmetric with respect to the emission angle. The emission occurs mainly in the polarization direction and the emission for small energies is favored. In the relativistic case the distribution is shifted in the laser propagation direction and becomes asymmetric. Moreover, the kinetic energy dependence on the emission angle becomes parabolic, which also follows from the simple classical dynamics at high intensities in Eq. (2): $\theta \sim A(\eta_0)$ and $\varepsilon_{kin} \sim A(\eta_0)^2$. However, the width of the energy and angular distribution remains almost the same as in the nonrelativistic case because the momentum spreading due to the field remains nonrelativistic: $\delta p = \sqrt{3\hbar\omega m/\gamma^3} \ll mc$ [25]. The dependence of the angular distribution of directly ionized electrons on the laser intensity offers a possibility to measure the laser intensity in the relativistic regime (see [33] and Section 2.2).

The low-energy spectrum of direct electrons integrated over all emission directions has no distinguished relativistic features and the dipole approximation results mainly coincide with the relativistic SFA calculations [34]. This is because the portion of the wave packet that tunnels out of the barrier in the considered relativistic regime is well described by the nonrelativistic approximation, since relativistic corrections to the bound state dynamics of the electron become important at $I > 10^{20}$ W/cm^2. Only the action of the laser field after the ionization step yields different angular distributions in the nonrelativistic and the relativistic treatments, leaving the total rate of the direct ionization unchanged.

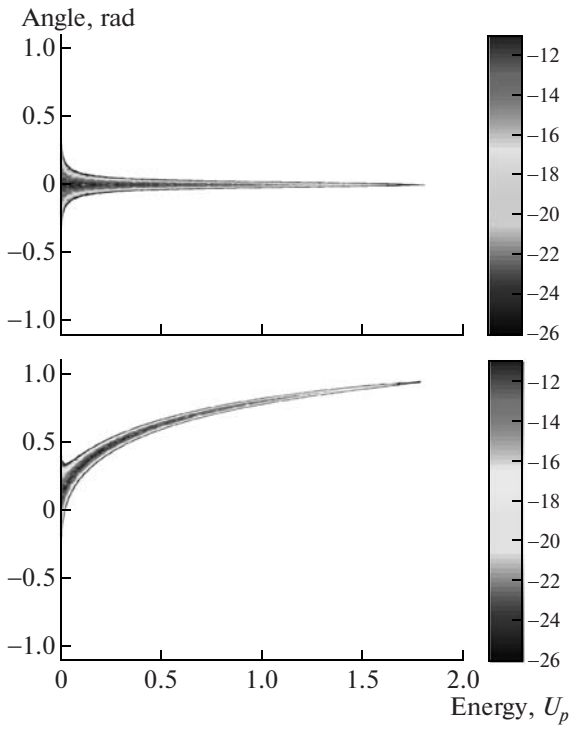

Fig. 1. Spectrum of a directly ionized electron, depending on the final energy in units of U_p and the emission angle θ (at $\phi = 0$), via $\log_{10}(dw_{\mathbf{p}}/d\Omega)$: (a) Schrödinger equation within the dipole approximation; (b) Klein–Gordon equation. The parameters of the driving laser field as well as of the atom are: intensity $I = 1.4 \times 10^{19}$ W/cm^2, angular frequency $\omega = 0.05$ au (corresponding to $U_p = 4 \times 10^4$ au $\approx 2.1mc^2$) and ionization potential $I_p = 32$ au (O^{7+}).

In contrast with the low-energy part, relativistic features arise in the plateau part of the spectrum where the recollision is responsible. In the relativistic case, the plateau is bended, has no interfering structure and is suppressed by magnitude, which all are due to the relativistic drift of the electron in the laser propagation direction [34]. The most interesting relativistic signatures for the rescattered electrons are seen in the angular distribution. Again the classical description indicates how the angular distribution of the rescattered electrons will be modified. Thus, the classical relativistic equations of motion yield the election energy and momenta after the interaction for the electron rescattered at the moment η_0:

$$p_x = p_{x0} + eA(\eta_0)/c\,, \qquad p_z = \frac{[p_{x0} + eA(\eta_0)/c]^2 - p_{x0}^2}{2\Lambda} + p_{z0}\,, \tag{3}$$

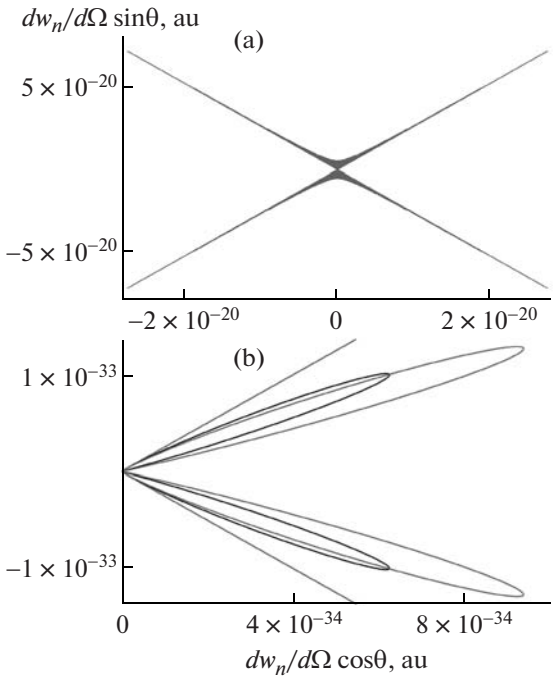

Fig. 2. Polar plots of the angular distribution for a final electron energy of $9U_p$, with a laser intensity of 2.6×10^{17} W/cm^2, an angular frequency of $\omega = 0.05$ au (equals $U_p = 750$ au) and an ionization potential of $I_p = 9.53$ au (B^{3+}): (gray) Schrödinger equation within the dipole approximation, (blue, the darkest) Schrödinger equation with magnetic field corrections and the relativistic mass shift, (red) Klein–Gordon equation. $\theta = 0$ corresponds to the direction of the laser polarization.

$$\varepsilon = c\frac{[p_{x0} + eA(\eta_0)/c]^2 - p_{x0}^2}{2\Lambda} + \varepsilon_0,$$

where ε_0, p_0 are the energy and momentum of the electron immediately after the rescattering, and $\Lambda = \varepsilon_0/c - p_{z0}$ is the integral of motion. The scattering angle at a given final electron energy $\varepsilon = \epsilon U_p$ will be maximal when the recolliding electron has the maximal energy, i.e., $A(\eta_0) = -a_0 mc^2$. Then,

$$p_x = p_{x0} + a_0 mc; \quad p_z = \frac{\epsilon - 3}{4} a_0^2 mc + p_{z0}, \qquad (4)$$

and the maximal rescattering angle with respect to the polarization direction is determined from the following equation

$$\cos\theta + \frac{\epsilon - 3}{4} a_0 \sin\theta = \frac{\sqrt{2}}{\sqrt{\epsilon}} \frac{\epsilon - 1 + \epsilon(\epsilon - 3)a_0^2/4}{4\sqrt{1 + \epsilon a_0^2/8}}. \qquad (5)$$

In the nonrelativistic case, $a_0 \ll 1$, there are two symmetric solutions of Eq. (5), $\theta = \pm\theta_d$, corresponding to two possible symmetric values for p_z. In the relativistic case, $\theta = \pm\theta_d + \delta$, i.e., the maximal electron emission angle of the rescattered electron is tilted towards the laser propagation direction. In the weakly relativistic regime, $\delta \approx (\epsilon - 3)a_0/4$.

The change in the angular distribution of the rescattered electrons due to relativistic effects is observable only in the weakly relativistic regime because otherwise the rescattering probability is negligible. Figure 2 displays the photoelectron angular distribution with a final electron energy of $9U_p$ in the case of 2.6×10^{17} W/cm^2 laser intensity, which is calculated using SFA based on the Klein–Gordon equation. The angular distribution is in general tilted towards the laser propagation direction. The new feature is that the side-lobes in backward direction, which arise due to the ionization rate increase near the cutoff energy, vanish (cf. Fig. 2b in comparison with Fig. 2a).

2.2. Relativistic Ionization beyond the Above-Threshold Regime

When the laser intensity is high enough such that $\gamma \ll 1$ the ionization takes place via tunneling which can be correctly described only quantum mechanically. At even higher intensities, the laser field strength can exceed the nuclear Coulomb field experienced by the atomic electrons. Then the potential barrier is completely suppressed and the electron may leave the bound state without the necessity of quantum tunneling. Over-barrier ionization (OBI) can therefore be described by classical means to a large extent as far as the probability of the quantum over-barrier reflection is negligible. The latter can be valid for intensities larger than the threshold intensity of OBI.

With next-generation laser sources, extremely relativistic intensities on the order of $I \sim 10^{23}$–10^{26} W/cm^2 are envisaged [35], reaching substantially beyond the maximum intensity of $I \approx 10^{22}$ W/cm^2 available at present [36]. They hold prospects to test the validity of QED through vacuum polarization [37], to study nuclear interactions [38] or to generate highly energetic particle beams which can be applied in medical situations such as treating cancer, for instance [39]. It is interesting to realize that measuring these ultrastrong relativistic intensities is not straightforward, as they exceed the damage-threshold of the detectors involved so that the standard method of simply recording the laser power and beam spot size becomes unfeasible. Relativistic OBI offers a solution to this practical problem [33]. Light atoms are not very useful, though, because they are fully ionized at such ultra-high intensities: the binding potential is quickly suppressed all the way to the 1s ground-state energy level. Rather hydrogen-like highly charged ions with nuclear charge number as high as $Z \sim 40$–50 are able to sustain these laser powers, at least for a while. Since their ionization rate strongly depends on the applied field, its measurement can be exploited to determine the unknown intensity. Ions can nowadays be generated in arbitrary

charge states with high purity and span a wide range of atomic field strengths [40], which renders them applicable to probe a correspondingly wide range of laser intensities.

OBI is the most suitable regime for this application, as the slope of the ionization rate as a function of the laser intensity is steepest there. This is illustrated in Fig. 3 where the laser intensity dependence of the ionization probability is shown for highly charged ions of various charge numbers. The curves were obtained by a classical Monte Carlo simulation, solving the classical relativistic equations of motion for an ensemble of electrons in the combined field of a Coulomb potential and a short laser pulse. The initial electron positions $\mathbf{r}_i$ and momenta $\mathbf{p}_i$ were distributed microcanonically. After the laser pulse has been switched off, an electron is counted as ionized when its final energy $\varepsilon_f = (\gamma_f - 1)mc^2 - Ze^2/|\mathbf{r}_f|$ is positive, where $\gamma_f = \sqrt{1 + |\mathbf{p}_f|^2/m^2c^2}$ is the electron Lorentz factor. For an approximated laser intensity range, an ion should be selected with maximal ascent at such intensities. Figure 3 indicates that laser intensities of around 10^{23} W/cm^2 may be sensitively measured by ions of $Z \approx 30$, whereas for near-future intensities in the range of 10^{24}–10^{25} W/cm^2 ions with charge $Z \approx 40$–60 are most suitable.

Apart from the total ionization yield, also the electron emission angle is a sensitive measure of the ionizing laser field strength [33] due to the relativistic effects outlined in Section 2.1.

3. ABOVE-THRESHOLD PAIR PRODUCTION

In very strong laser fields electron-positron (e^+e^-) pairs can be produced. This has been demonstrated experimentally at SLAC where positrons were detected after the collision of an ultrarelativistic electron beam with an intense optical laser pulse [32]. As mentioned in the introduction, strong-field pair production shares common features with atomic ionization. In the multiphoton domain with $\xi \ll 1$, the production probability follows a perturbative power law, $W \sim \xi^{2n_0}$, where n_0 denotes the minimal number of laser photons required from energy conservation in the process. In the tunneling regime with $\xi \gg 1$, the probability shows an exponential scaling, $W \sim \exp(-\pi E_c/E)$, where $E_c = m^2c^3/e\hbar$ denotes the QED critical field [41]. The SLAC experiment observed pair production in the multiphoton regime through the nonlinear Breit-Wheeler reaction $\omega_\gamma + n\omega \longrightarrow e^+e^-$ where a high-energy γ-photon combines its energy with n laser photons to produce the pair [42]. The γ-photon was generated by Compton backscattering of a laser photon off the ultrarelativistic electron beam. In the following we consider two different processes of pair production in the above-threshold regime ($\xi \sim 1$).

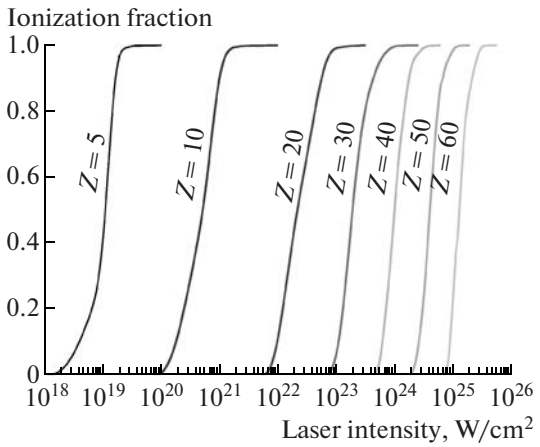

Fig. 3. Ionization fraction for different hydrogen-like ions with nuclear charge Z as a function of the maximal laser intensity for a single-cycle sinusoidal square-shaped laser pulse with a photon energy of $\hbar\omega = 1.6$ eV.

3.1. Pair Production in Combined Laser and Nuclear Coulomb Fields

Another mechanism than in the SLAC experiment is responsible for pair creation when a heavy projectile like a nucleus collides with a laser field. Here the particles are generated via a virtual photon from the nuclear Coulomb field (nonlinear Bethe–Heitler process [28]). Because of the large projectile mass the two-step Breit–Wheeler process via Compton scattering is suppressed. Starting with the early work of Yakovlev [43], several theoreticians have studied nonlinear Bethe–Heitler pair creation, with a focus on the tunneling and multiphoton regimes of interaction (see [44–50] and references therein). Relatively little work has been done on the intermediate above-threshold regime where $\xi \sim 1$ [45, 46]. It could be realized in the head-on collision of (a) a relativistic nucleus (Lorentz factor $\gamma_p \sim 10^2$) with a tightly focused X-ray laser beam ($\hbar\omega_0 \sim 1$ keV, $I \sim 10^{24}$ W/cm^2 [51, 52]) or (b) an ultrarelativistic proton ($\gamma_p \sim 10^4$ [53]) with an intense optical laser pulse ($\hbar\omega_0 \sim 1$ eV, $I \sim 10^{18}$ W/cm^2). Within the framework of the relativistic SFA [42, 43], we have numerically calculated the total rate for nonlinear Bethe–Heitler pair production in the above-threshold domain. Proton impact on a monochromatic laser wave of circular polarization with $\xi = 1$ was assumed. Over the spins and momenta of the outgoing particles has been summed and integrated, respectively. Our results are shown in Fig. 4. The minimal number of photons to produce a pair is given by

$$n_0 = \frac{2m_*c^2}{\hbar\omega}, \tag{6}$$

where $m_* = m\sqrt{1+\xi^2} = \sqrt{2}m$ is the laser-dressed electron mass and $\omega \approx 2\gamma_p\omega_0$ the laser frequency in the

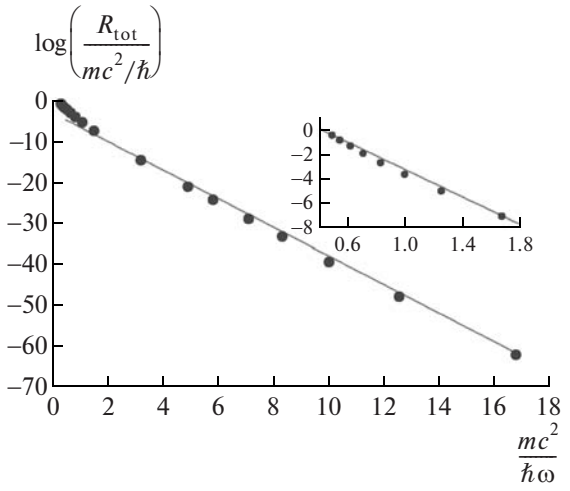

Fig. 4. Total rate for ATPP at $\xi = 1$ in the proton frame, as a function of the laser frequency. The dots show numerical data from an SFA calculation, the solid line is the analytical fit function of Eq. (7). The inset shows an enlargement of the high-frequency region where the frequency scaling is modified.

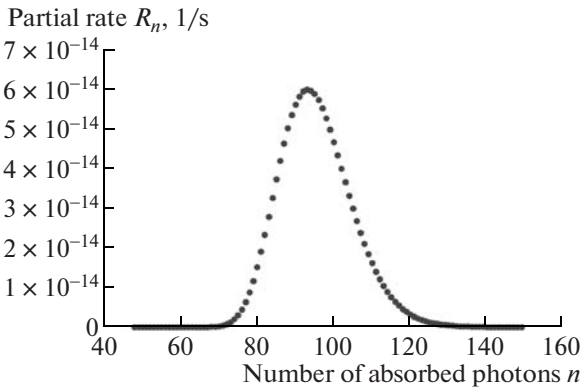

Fig. 5. Partial rates for ATPP as a function of the absorbed photon number. The Doppler-shifted photon energy is $\hbar\omega = 30$ keV in the rest frame of the projectile proton which impacts the laser beam.

projectile frame. For the collision scenarios outlined above, the latter is of the order of $\hbar\omega \sim 100$ keV. While in the multiphoton and tunneling regimes, closed-form expressions for the total pair creation rate can be derived by analytical means (see, e.g., [47]), for ATPP corresponding formulas are not known. We have therefore fitted an analytical curve to our numerical data. This way we obtain the approximate scaling relation

$$R_{\mathrm{tot}} \sim \exp\left(-3.49\frac{mc^2}{\hbar\omega}\right) \tag{7}$$

for the total ATPP rate in the frequency range $30\ \mathrm{keV} \le \hbar\omega \le 300$ keV. The relative error of the numerical constant in the exponent amounts to 1%. The exponential behavior in Eq. (7) closely resembles the pair production rate in the tunneling regime which scales as $\sim\exp(2\sqrt{3}E_c/E)$ in combined laser and nuclear fields [47]; note that $E_c/E = mc^2/\hbar\omega\xi$. ATPP at low laser frequencies $\hbar\omega \ll mc^2$ in the projectile frame is therefore heavily suppressed. At high frequencies the rate scaling is modified to $R_{\mathrm{tot}} \sim \exp(-5.57mc^2/\hbar\omega)$, with a 3% error in the numerical constant (see the inset in Fig. 4). We have also analyzed the region of photon numbers which are mainly contributing to ATPP. Within the same frequency range as shown in Fig. 4, the mean photon number is proportional to the minimal photon number and given by

$$\bar{n} \approx 1.9n_0. \tag{8}$$

The proportionality between $\bar{n}$ and n_0 is in accordance with the results in [43]. Similar to ATI, the typical number of absorbed photons is considerably larger than n_0.

For example, for $\hbar\omega = 30$ keV, we obtain $n_0 = 49$ and $\bar{n} = 94$ (see Fig. 5). The width of the photon number distribution decreases when the laser frequency increases according to the fit function

$$\Delta n \approx 5.1\left(\frac{n_0 mc^2}{\hbar\omega}\right)^{0.21}, \tag{9}$$

with a relative error of 1.5% in the exponent and 1% in the numerical prefactor. The photon number distribution resembles the energy spectrum of the created particles since $n\hbar\omega = q_+^0 + q_-^0$, with the quasi-energies $q_\pm^0$ of the $e^\pm$. An analysis by analytical means shows that the most probable polar emission angle of the particles amounts to

$$\theta_\pm = \arctan\frac{m_* c}{|\mathbf{q}_\pm|} \tag{10}$$

in the nuclear rest frame.

Let us compare the peak of the electron spectrum determined numerically by Eq. (8) for $\xi = 1$ and the most probable angle of the electron emission in Eq. (10) with the corresponding quantities for ATI. The latter is well reproduced by the classical mechanical estimation derived from the electron dynamics in the laser field. Therefore, we return to Eq. (1) and calculate the electron quasi-energy (q_0) and quasi-momentum ($\mathbf{q}$) as a cycle average of the electron energy and momentum in the laser field:

$$\begin{aligned} q_\perp &= \frac{e}{c}A(\eta_0); \\ q_z &= \frac{e^2}{2mc^3}[A(\eta_0)^2 + \overline{A(\eta)^2}]; \\ q_0 &= mc^2 + \frac{e^2}{2mc^3}[A(\eta_0)^2 + \overline{A(\eta)^2}], \end{aligned} \tag{11}$$

where the overbar indicates the cycle averaging. In a circularly polarized laser field, the electron will be mainly produced with the following quasi-energy and momentum

$$q_\perp = mc\xi; \quad q_z = mc\xi^2; \quad q_0 = mc^2(1+\xi^2). \quad (12)$$

This implies $|\mathbf{q}| = m_* c\xi$ and the condition of Eq. (10) is recovered: $\tan\theta = q_\perp/q_z = 1/\xi$. The classical estimate for the most probable photon number is $\bar{n} = 2q_0/\hbar\omega = 2mc^2(1+\xi^2)/\hbar\omega = n_0\sqrt{1+\xi^2} = \sqrt{2}n_0$ in the case of $\xi = 1$, which does not differ significantly from that of the numerical calculation in Eq. (8). The difference is caused by the fact that in Eq. (8) the electron momentum has been integrated over, whereas the classical estimate refers to a certain momentum value. We may conclude that, surprisingly, the maximum of the electron spectrum and of the emission angle for pair production in laser and Coulomb fields is well reproduced by our classical mechanical estimations and is similar to that for ATI.

With respect to the linear Bethe–Heitler effect by a single high-energy photon, we point out that the influence of a strong low-frequency background laser field ($\xi \approx 10$) on this process has recently been studied [54]. Moreover, nonlinear Bethe–Heitler creation of muon pairs has been considered in the multiphoton regime [55].

3.2. Pair Production in Counterpropagating Laser Pulses

In this section, pair production from vacuum in the field of two counterpropagating laser beams is investigated. In the laser-ion collisions of the previous section, the Doppler boost of the laser parameters due to a highly relativistic Lorentz factor can be exploited. In "laser-laser collisions" this is not possible so that high laser frequencies and/or field strengths are required to exist in the laboratory frame. During recent years there has been an enormous progress in laser technology and further advances are envisaged [35, 36], so that an experimental observation of pair creation in pure laser fields is indeed coming into reach [51, 56]. Note that a single plane-wave laser field cannot extract pairs from the vacuum due to energy and momentum conservation. We have studied pair creation in two counterpropagating, linear-polarized laser pulses of equal frequency and intensity, focusing on the nonperturbative regime with $\xi = 1$ (for both laser beams taken together). The formation length scale for tunneling pair creation is $l \sim 2mc^2/eE = \lambda_C E_c/E$. For small laser frequencies, $\omega \ll (mc^2/\hbar)(E_c/E)$ (or $\xi \gg 1$), one can usually neglect the spatial dependence of the applied field, arriving this way at a solely time-dependent, oscillating electric field. By applying this dipole approximation, we first derive some essential features of pair production in counterpropagating laser pulses, and afterwards describe modifications which arise at high laser frequencies when taking into account the spatial field dependence and the impact of the laser's magnetic-field component.

We study the process numerically, employing an advanced computer code which solves the Dirac equation in an arbitrary external potential on a two dimensional spatial grid by propagating an initial state via the split-operator algorithm [57]. In our case the initial state is given by a negative-energy Gaussian wave packet, representing an electron in the Dirac sea. Under the influence of the applied field the wave packet can undergo transitions to the positive-energy continuum. By projecting the final state onto all positive-energy states after the field has been switched off, the pair creation amplitude is obtained.

In the case of a space-independent oscillating electric field, momentum conservation reduces the problem to a two-level system consisting of a negative and a positive energy state coupled by the external field. Multiphoton resonances occur at certain frequencies, enforced by energy conservation

$$\omega_n = \frac{2q_0(\mathbf{p})}{n\hbar}. \quad (13)$$

Here, n denotes the number of absorbed photons needed to overcome the energy gap and $q_0(\mathbf{p}) = \frac{c}{T}\int_0^T dt \sqrt{m^2c^2 + \left(\mathbf{p} - \frac{e}{c}\mathbf{A}(t)\right)^2}$, is the quasi-energy of the laser dressed state, with the vector potential $\mathbf{A}(t)$, the pulse duration T, and the canonical momentum $\mathbf{p}$. For $\mathbf{p} = 0$ and $\xi = 1$, the value of the quasi-energy is $q_0(0) \approx 1.21mc^2$, independent of the field frequency. When the pulse length is varied at a resonance frequency, the transition amplitude undergoes Rabi oscillations [58], like in a quantum optical two-level system. An example is shown in Fig. 6 by the red solid curve, corresponding to an $n = 3$ photon resonance at frequency $\omega_3 = 0.833mc^2/\hbar$. For this example the chosen frequency is rather large, in order to reveal below the influence of the laser magnetic field component. We note moreover that, in the quasiclassical limit, the probability for ATPP in an oscillating electric field with $\xi = 1$ exhibits an exponential behavior

$$W \sim \exp\left(-\alpha\frac{mc^2}{\hbar\omega}\right), \quad (14)$$

with $\alpha \approx 3$, in close similarity with Eq. (7).

While pair creation in an oscillating electric field can also be treated by analytical means [59], our numerical apparatus gives us the possibility to take also the spatial dependence of the fields into account [60], which analytically is a very difficult problem [61]. Meanwhile, according to Eq. (14), significant ATPP probabilities require high laser frequency when usually

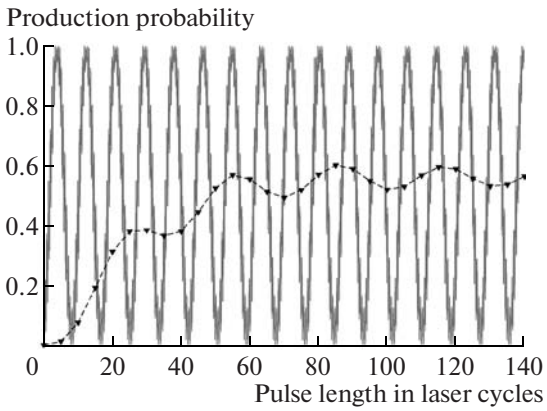

Fig. 6. Above-threshold pair production probability in counterpropagating laser beams, as a function of the pulse length ($\xi = 1$). The solid line shows the Rabi oscillation for the case of an oscillating electric field of frequency $\omega = 0.833mc^2/\hbar$, corresponding to an $n = 3$ photon resonance ($\mathbf{p} = 0$). The black triangles show the disturbed Rabi oscillation due to the magnetic component of the laser field. Here the 3-photon resonance frequency is shifted to $\omega = 0.855mc^2/\hbar$.

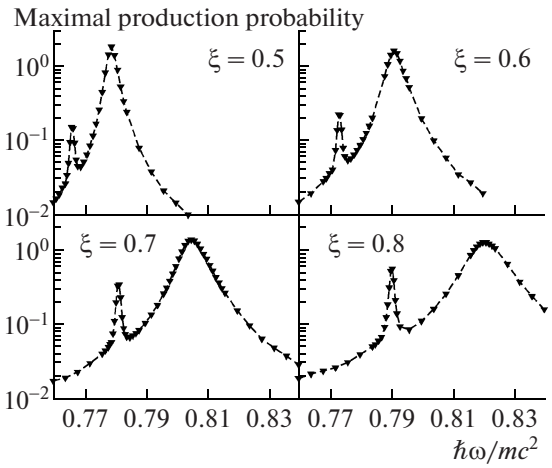

Fig. 7. Splitting of the $n = 3$ photon resonance peak for various values of ξ. Note that the position of the main resonance increases, in accordance with the ξ dependent enhancement of m_*. A quadratic curve fit yields $\Delta\omega = (0.043\xi^2 + 0.002)mc^2/\hbar$.

$\xi \lesssim 1$, and the effects from the laser magnetic field are expected to be pronounced.

Inclusion of the magnetic field strongly modifies the Rabi oscillation pattern, as shown in Fig. 6 by the black triangles. While the 3-photon resonance frequency is only slightly shifted to $\omega = 0.855mc^2/\hbar$, the Rabi flopping is significantly changed from the typical $\sin^2$ behavior to an oscillation around a plateau value and the Rabi frequency Ω_R is decreased approximately by a factor of 3.5. As before, we assume in our calculations a vanishing initial momentum, $\mathbf{p} = 0$, which however is not conserved any longer. Because of the magnetic field, the photons carry momentum in propagation direction (chosen as z axis). Therefore the energy-momentum conservation is given by

$$\begin{aligned} q_0' &= (n_+ + n_-)\hbar\omega - q_0, \\ q_3' &= (n_+ - n_-)\frac{\hbar\omega}{c} - q_3, \end{aligned} \tag{15}$$

where q and q' denote the quasi-energy-momentum four-vectors before and after the interaction. The integers n_+ and n_- denote the number of photons absorbed from the right and left traveling laser pulse, respectively. According to Eq. (15), the resonance condition in Eq. (13) is modified into

$$\omega_{n_+,n_-} = \frac{m_* c^2}{2\hbar}\frac{n_+ + n_-}{n_+ n_-}. \tag{16}$$

The value of the laser-dressed mass m_* (satisfying $q^2 = m_*^2 c^2$) was numerically determined as $m_* = 1.11m$; no analytical expression for the quasi-energy in this field configuration is known. For a certain multiphoton order there are now multiple resonance frequencies, e.g., for an $n = n_+ + n_- = 5$ photon transition there are two different resonance frequencies $\omega_{3.2}$ and $\omega_{4.1}$. The number of resonance lines is enhanced correspondingly. For the $n = 3$ photon resonance Eq. (16) predicts a unique frequency $\omega_{2.1}$, which however is not confirmed by the numerical results. Instead, for $n_+ \neq n_-$ the resonant peaks are always split into doublets, leading to a further enhancement of the number of resonance lines. This effect is not covered by Eq. (16) which rather predicts the center of the split lines. The emergence of the splitting is shown for the case of the $n = 3$ photon transition in Fig. 7 for increasing values of ξ. The keypoint to understand the splitting is again the photon momentum due to which the former two-level scheme is broken into a V-type three-level scheme: the initial negative-energy level and two positive-energy levels, having the same energy but opposite momentum. The upper two levels are coupled via Compton scattering, leading to a splitting of these levels and thus to a splitting $\Delta\omega$ of the resonant transition frequency, which depends quadratically on ξ. The splitting is analogous to the Autler–Townes effect.

Upcoming X-ray laser sources [51, 52] offer prospects to enter the parameter regime of interest for ATPP in counterpropagating laser pulses. The anticipated bandwidth of X-ray free-electron lasers [62] would be sufficient to resolve the influence of the magnetic field component onto the resonance spectrum, due to a change of the relative resonance line separation: While, like in Eq. (13), a relative separation of $\sim 1/n$ remains between resonance lines of different $n = n_+ + n_-$ values, the relative distance between the newly occurred resonance lines belonging to the same n value follows a $\sim 1/n^2$ behavior [see Eq. (16)].

4. CONCLUSIONS

In conclusion, we compare the relativistic strong-field ionization and pair production processes in the nonperturbative above-threshold regime which have been considered above. All these processes have in common that they occur in an intermediate regime of interaction, located between the perturbative multiphoton and the quasi-static tunneling domains. As a consequence, both the photon and the field nature of the external laser wave are of similar importance here. On the one hand, total ATI [12] and ATPP rates resemble the exponential behavior known from the tunneling regime where the field aspect dominates. On the other hand, photoelectron peaks in ATI spectra are separated by a photon energy, and electron peaks in ATPP spectra in counterpropagating laser pulses are separated by a photon momentum [60]. ATPP in laser and Coulomb fields does not exhibit this feature since the nucleus can absorb recoil momentum. A typical feature of all above-threshold phenomena is that more photons from the external laser field are absorbed than the minimal number required to surmount the respective energy gap. The energy and angle resolved spectra for ATPP in laser and Coulomb fields are very similar to those of ATI.

A major difference between ATI and ATPP in combined laser and Coulomb fields is the role played by recollisions. In the case of ATI, recollisions represent an important correlation effect which contributes to the plateau in the photoelectron spectrum. The Coulomb parameter Z/v, with the ionized electron velocity v, is relatively large in nonrelativistic or weakly relativistic ATI [8]. Recollisions have recently also been discussed in the context of strong-field pair production [49]: After their creation in a relativistic laser-ion collision, the electron and positron are driven by the laser field into a recollision which can induce secondary processes such as $e^+e^- \longrightarrow e^+e^-$ (electron-positron scattering), $e^+e^- \longrightarrow 2\gamma$ (electron-positron annihilation) or $e^+e^- \longrightarrow \mu^+\mu^-$ (muon pair creation; see also [63]). The Coulomb field responsible for the pair production is not involved in these subsequent processes, though, in contrast to the recollision phenomena in atomic physics. The reason is, that the Coulomb parameter in the case of pair production, Z/c, is usually small, suppressing the importance of electron-ion correlation effects.

Relativistic above-threshold phenomena are interesting both for nonperturbative quantum theory and intense femtosecond laser experiments. In particular, relativistic strong-field ionization of highly charged ions could be applied as a sensitive probe of super-high intensities in excess of 10^{23} W/cm^2 at upcoming laser facilities. Even higher laser intensities close to the Schwinger limit might be measurable via pair creation processes.

ACKNOWLEDGMENTS

We acknowledge the help of M. Klaiber in the calculations presented in Section 2.1.

REFERENCES

1. N. B. Delone and V. P. Krainov, *Multiphoton Processes in Atoms* (Springer, Berlin, 1994).
2. N. B. Delone and V. P. Krainov, *Nonlinear Ionization of Atoms by Laser Radiation* (Fizmatlit, Moscow, 2001) [in Russian].
3. N. B. Delone, *Interaction of Laser Radiation with Matter* (Nauka, Moscow, 1989) [in Russian].
4. N. B. Delone and M. V. Fedorov, Prog. Quant. Electron. **13**, 267 (1989).
5. M. V. Fedorov, *Atomic and Free Electrons in a Strong Light Field* (World Sci., Singapore, 1997).
6. P. Agostini, F. Fabre, G. Mainfray, et al., Phys. Rev. Lett. **42**, 1127 (1979).
7. V. S. Popov, Zh. Eksp. Teor. Fiz. **63**, 1586 (1972) [Sov. Phys. JETP **36**, 840 (1973)].
8. V. I. Ritus, J. Rus. Laser Res. **6**, 497 (1985); see p. 36.
9. S. P. Goreslavsky, N. B. Delone, and V. P. Krainov, Sov. Phys. JETP **55**, 1032 (1982) [Zh. Eksp. Teor. Fiz. **82**, 1789 (1982)]; N. B. Delone, S. P. Goreslavsky, and V. P. Krainov, J. Phys. B **27**, 4403 (1994).
10. L. V. Keldysh, Zh. Eksp. Teor. Fiz. **47**, 1945 (1964) [Sov. Phys. JETP **20**, 1307 (1965)].
11. A. M. Perelomov, V. S. Popov, M. V. Terentyev, Sov. Phys. JETP **23**, 924 (1966); Sov. Phys. JETP **24**, 207 (1967); Sov. Phys. JETP **25**, 336 (1967).
12. M. V. Ammosov, N. B. Delone, and V. P. Krainov, Zh. Eksp. Theor. Fiz. **91**, 2008 (1986) [Sov. Phys. JETP **64**, 1191 (1986)].
13. F. H. M. Faisal, J. Phys. B **6**, L312 (1973); H. R. Reiss, Phys. Rev. A **22**, 1786 (1980).
14. W. Becker, F. Grasbon, R. Kopold, et al., Adv. At. Mol. Opt. Phys. **48**, 35 (2002); D. B. Milosević, G. G. Paulus, D. Bauer, and W. Becker, J. Phys. B **39**, R203 (2006).
15. Y. I. Salamin, S. X. Hu, K. Z. Hatsagortsyan, and C. H. Keitel, Phys. Rep. **427**, 41 (2006); G. A. Mourou, T. Tajima, and S. V. Bulanov, Rev. Mod. Phys. **78**, 309 (2006).
16. M. Dammasch, M. Dörr, U. Eichmann, et al., Phys. Rev. A **64**, 061402(R) (2001).
17. S. Palaniyappan, I. Ghebregziabher, A. DiChiara, et al., Phys. Rev. A **74**, 033403 (2006).
18. M. Klaiber, K. Z. Hatsagortsyan, and C. H. Keitel, Phys. Rev A **71**, 033408 (2005).
19. S. X. Hu and C. H. Keitel, Phys. Rev A **63**, 053402 (2001).
20. F. H. M. Faisal and S. Bhattacharyya, Phys. Rev. Lett. **93**, 053002 (2004).
21. H. R. Reiss, Phys. Rev. A **42**, 1476 (1990); J. Opt. Soc. Am. B **7**, 574 (1990).
22. D. P. Crawford and H. R. Reiss, Phys. Rev. A **50**, 1844 (1994); Opt. Expr. **2**, 289 (1998).
23. V. S. Popov, V. D. Mur, and B. M. Karnakov, JETP Lett. **66**, 229 (1997); V. D. Mur, B. M. Karnakov, and

V. S. Popov, JETP **87**, 433 (1998); V. S. Popov, B. M. Karnakov, and V. D. Mur, JETP Lett. **79**, 262 (2004).

24. N. Milosević, V. P. Krainov, and T. Brabec, Phys. Rev. Lett. **89**, 193001 (2002); J. Phys. B **35**, 3515 (2002).
25. V. P. Krainov and S. P. Roshchupkin, J. Opt. Soc. Am. B **9**, 1231 (1992); V. P. Krainov, Opt. Express **2**, 268 (1998); S. P. Goreslavsky and S. V. Popruzhenko, Opt. Express **2**, 271 (1998); V. P. Krainov, J. Phys B **32**, 1607 (1999); J. Phys B **36**, L169 (2003); V. P. Krainov and A. V. Sofronov, Phys. Rev. A **69**, 015401 (2004); Phys. Rev. A **77**, 063418 (2008).
26. A. D. DiChiara, I. Ghebregziabher, R. Sauer, et al., Phys. Rev. Lett. **101**, 173002 (2008).
27. S. Palaniyappan, R. Mitchell, R. Sauer, et al., Phys. Rev. Lett. **100**, 183001 (2008).
28. H. A. Bethe and W. Heitler, Proc. Roy. Soc. London A **146**, 83 (1934).
29. J. Eichler, Phys. Rep. **193**, 165 (1990); G. Baur, K. Hencken, and D. Trautmann, Phys. Rep. **453**, 1 (2007).
30. G. P. Adams, Phys. Rev. **74**, 1707 (1948).
31. Bethe-Heitler pair creation in a high-Z target via bremsstrahlung photons from laser-accelerated electrons has been observed in C. Gahn et al., Appl. Phys. Lett. **77**, 2662 (2000); Phys. Plasmas **9**, 987 (2002).
32. D. Burke, R. C. Field, G. Horton-Smith, et al., Phys. Rev. Lett. **79**, 1626 (1997).
33. H. G. Hetzheim and C. H. Keitel, Phys. Rev. Lett. **102**, 083003 (2009).
34. M. Klaiber, K. Z. Hatsagortsyan, and C. H. Keitel, Phys. Rev. A **75**, 063413 (2007).
35. European Light Infrastructure (ELI), ELI Scientific Case, http://www.extreme-light-infrastructure.eu/; High Power laser Energy Research (HiPER), HiPER Technical Background and Conceptual Design Report, http://www.hiperlaser.org/docs/tdr/HiPERTDR2.pdf.
36. S. W. Bahk, P. Rousseau, T. A. Planchon, et al., Opt. Lett. **29**, 2837 (2004); Y. Yanovsky, V. Chvykov, G. Kalinchenko, et al., Opt. Express **16**, 2109 (2008).
37. G. Brodin, M. Marklund, and L. Stenflo, Phys. Rev. Lett. **87**, 171801 (2001); T. Heinzl, B. Liesfeld, K.-U. Amthor, et al., Opt. Commun. **267**, 318 (2006); A. Di Piazza, K. Z. Hatsagortsyan, and C. H. Keitel, Phys. Rev. Lett. **97**, 083603 (2006); Phys. Rev. Lett. **100**, 010403 (2008).
38. G. Pretzler, A. Saemann, A. Pukhov, et al., Phys. Rev. E **58**, 1165 (1998); K. W. D. Ledingham, I. Spencer, T. McCanny, et al., Phys. Rev. Lett. **84**, 899 (2000); T. J. Bürvenich, J. Evers, and C. H. Keitel, Phys. Rev. Lett. **96**, 142501 (2006).
39. S. Fritzler, V. Malka, G. Grillon, et al., Appl. Phys. Lett. **83**, 3039 (2003); H. Schwoerer, S. Pfotenhauer, O. Jäckel, et al., Nature (London) **439**, 445 (2006); Y. I. Salamin, Z. Harman, and C. H. Keitel, Phys. Rev. Lett. **100**, 155004 (2008).
40. P. H. Mokler and Th. Stöhlker, Adv. At. Mol. Opt. Phys. **37**, 297 (1996); J. Ullrich, R. Moshammer, R. Dörner, et al., J. Phys. B **30**, 2917 (1997); J. R. C. López-Urrutia, J. Braun, G. Brenner, et al., J. Phys. Conf. Ser. **2**, 42 (2004).
41. J. Schwinger, Phys. Rev. **82**, 664 (1951).
42. H. R. Reiss, J. Math. Phys. **3**, 59 (1962); Phys. Rev. Lett. **26**, 1072 (1971); V. I. Ritus, Nucl. Phys. B **44**, 236 (1972).
43. V. P. Yakovlev, Zh. Eksp. Teor. Fiz. **49**, 318 (1965) [Sov. Phys. JETP **22**, 223 (1966)].
44. S. P. Roshchupkin, Laser Phys. **6**, 837 (1996).
45. C. Müller, A. B. Voitkiv, and N. Grün, Phys. Rev. A **70**, 023412 (2004).
46. H. K. Avetissian, A. K. Avetissian, G. F. Mkrtchian, and K. V. Sedrakian, Nucl. Instrum. Methods Phys. Res. A **507**, 582 (2003).
47. A. I. Milstein, C. Müller, K. Z. Hatsagortsyan, et al., Phys. Rev. A **73**, 062106 (2006).
48. J. Z. Kaminski, K. Krajewska, and F. Ehlotzky, Phys. Rev. A **74**, 033402 (2006); K. Krajewska and J. Z. Kaminski, Laser Phys. **18**, 185 (2008).
49. M. Yu. Kuchiev, Phys. Rev. Lett. **99**, 130404 (2007).
50. C. Müller, Phys. Lett. B **672**, 56 (2009).
51. A. Ringwald, Phys. Lett. B **510**, 107 (2001).
52. G. D. Tsakiris, K. Eidmann, J. Meyer-ter-Vehn, and F. Krausz, New J. Phys. **8**, 19 (2006).
53. *The LHC Design Report*, Ed. by O. Brüning, et al., CERN Report No. 2004-003, http://lhc.web.cern.ch.
54. E. Lötstedt, U. D. Jentschura, and C. H. Keitel, Phys. Rev. Lett. **101**, 203001 (2008); New J. Phys. **11**, 013054 (2009).
55. C. Müller, C. Deneke, and C. H. Keitel, Phys. Rev. Lett. **101**, 060402 (2008).
56. R. Alkofer, M. B. Hecht, C. D. Roberts, et al., Phys. Rev. Lett. **87**, 193902 (2001); M. V. Fedorov, M. A. Efremov, and P. A. Volkov, Opt. Comm. **264**, 413 (2006); S. S. Bulanov, N. B. Narozhny, V. D. Mur, and V. S. Popov, Zh. Eksp. Teor. Fiz. **129**, 14 (2006) [JETP **102**, 9 (2006)]; C. C. Gerry, Q. Su, and R. Grobe, Phys. Rev. A **74**, 044103 (2006); Q. Su and R. Grobe, Laser Phys. **17**, 92 (2007).
57. G. R. Mocken and C. H. Keitel, Comput. Phys. Comm. **178**, 868 (2008).
58. V. S. Popov, Pis'ma Zh. Eksp. Teor. Fiz. **18**, 435 (1973) [JETP Lett. **18**, 255 (1973)]; V. M. Mostepanenko and V. M. Frolov, Yad. Fiz. **19**, 885 (1974) [Sov. J. Nucl. Phys. **19**, 451 (1974)]; H. K. Avetissian, A. K. Avetissian, G. F. Mkrtchian, and Kh. V. Sedrakian, Phys. Rev. E **66**, 016502 (2002).
59. E. Brezin and C. Itzykson, Phys. Rev. D **2**, 1191 (1970); V. S. Popov, JETP Lett. **13**, 185 (1971).
60. M. Ruf, G. R. Mocken, C. Müller, K. Z. Hatsagortsyan, and C. H. Keitel, Phys. Rev. Lett. **102**, 080402 (2009).
61. H. Gies and K. Klingmüller, Phys. Rev. D **72**, 065001 (2005); G. V. Dunne and C. Schubert, Phys. Rev. D **72**, 105004 (2005).
62. M. Altarelli, R. Brinkmann, M. Chergui, et al., *Technical Design Report of the European XFEL*, DESY 2006-097, http://www.xfel.net.
63. C. Müller, K. Z. Hatsagortsyan, and C. H. Keitel, Phys. Lett. B **659**, 209 (2008); Phys. Rev. A **78**, 033408 (2008); I. Kuznetsova, D. Habs, and J. Rafelski, Phys. Rev. D **78**, 014027 (2008).